Hindawi
International Journal of Photoenergy
Volume 2019, Article ID 5783507, 11 pages
https://doi.org/10.1155/2019/5783507

Research Article

Influence of the Textural Parameters of LDH-TiO_2 Composites on Phenol Adsorption and Photodegradation Capacities

J. C. Contreras-Ruiz,[1] S. Martínez-Gallegos,[1] J. L. García-Rivas,[1] J. Illescas,[1] J. C. González-Juárez,[1] Guadalupe Macedo Miranda,[1] and Eduardo Ordoñez Regil[2]

[1]*Instituto Tecnológico de Toluca, Av. Instituto Tecnológico s/n, Colonia Agrícola Bellavista, Metepec, Edo. de México 52149, Mexico*
[2]*Departamento de Química, Instituto Nacional de Investigaciones Nucleares, A.P. 17-1027. Col. Escandón, Delegación Miguel Hidalgo 11801, Mexico City, Mexico*

Correspondence should be addressed to S. Martínez-Gallegos; soniazteca@hotmail.com

Received 6 July 2018; Revised 3 October 2018; Accepted 18 October 2018; Published 6 January 2019

Academic Editor: Adel A. Ismail

Layered double hydroxides (LDH) $M^{2+}M^{3+}CO_3^{2-}$ were synthesized following the sol-gel methodology using Mg-Al, Mg-Fe, and Zn-Al as cation pairs for subsequent use in the preparation of TiO_2/LDH materials. The samples were characterized by infrared spectroscopy (IR), scanning electron microscopy (SEM), and the Brunauer–Emmett–Teller (BET) technique to determine the surface area (SA); the results of which were used to determine the roughness of the samples in terms of surface fractal dimension (D). The prepared materials exhibited both adsorption and photocatalytic properties in the removal of phenol in aqueous solution under ultraviolet irradiation. This work studies the relationship between the textural parameters of the materials obtained in relation to their photocatalytic efficiency and adsorption capacity, finding that the surface of the solids, their structural heterogeneity, and roughness condition the photodegradation and adsorption processes, using phenol as reference organic pollutant. The results show that different cation in LDH influences in photocatalytic capacity; the TiO_2/ZnAl was the best material in one test, but after 10 times of test, the TiO_2/MgFe gave the better photodegradation material. In adsorption capacity, TiO_2/ZnAl and TiO_2/MgFe have a close rate for phenol adsorption and both were better than TiO_2/MgAl. The differences in textural characteristics (surface area, surface roughness, and pore-size distribution) affected phenol adsorption and photodegradation efficiency.

1. Introduction

TiO_2 is the most attractive material used in the photocatalytic degradation of toxic organic compounds in water due, to a large extent, to the generation of highly oxidant species ($^{\cdot}OH$ radicals). These species have high catalytic activity, with a broad valence band (3.0–3.2 eV), low toxicity, and good resistance to mild chemical corrosion [1–5]. The many methods for preparing TiO_2 include sol-gel [6], hydrothermal, chemical and physical vapor deposition [7], chloride process, impregnation, coprecipitation, direct oxidation of $TiCl_4$, or through the calcination of organic precursors such as titanium isopropoxide [8, 9]. The textural characteristics of TiO_2 depend on the calcination temperature used during synthesis; the temperature range from 500 to 650°C was found to produce materials with better photocatalytic properties [1, 10, 11]. Furthermore, the size of commercial TiO_2 particles is usually nanometric, making postuse recovery of the photocatalyst difficult, in addition to causing accumulation or blocking in the equipment, thus limiting its practical application. Various attempts have been made to improve the photoactivity of TiO_2 by the addition of adsorbents such as silica, alumina, zeolites, clays, and activated carbon [12–15]. A suitable material for immobilizing TiO_2 particles is the anionic clay family known as layered double hydroxides (LDH). LDH are porous materials with a large surface area and good adsorption capacity for organic pollutants and many surface hydroxyl groups, as well as being excellent dispersants and carriers for TiO_2 particles to produce materials with photocatalytic properties in the phenol

removal [16–20]. LDH structure is described based on the distribution of magnesium hydroxide $Mg(OH)_2$, where the base units are sheets with Mg^{2+} cations located in the center, in octahedral coordination by OH^- groups. Each Mg^{2+} cation shares its charges with six OH^- anions. LDH are the result of the isomorphic substitution of a fraction of the Mg^{2+} cations by a trivalent cation (M^{3+}), thereby generating a positive charge residue which is offset by the presence of intercalated anions [21]. The general formula for LDH is $[M^{2+}_{1-x}\ M^{3+}_{x}\ (OH)_2]^{x+}\ (A^{n-})_{x/n}\cdot mH_2O$, where M^{2+} is a divalent cation (Ca^{2+}, Mg^{2+}, Zn^{2+}, Co^{2+}, Ni^{2+}, Cu^{2+}, Mn^{2+}), M^{3+} is a trivalent cation (Al^{3+}, Cr^{3+}, Fe^{3+}, Co^{3+}, Ni^{3+}, Mn^{3+}); A^{n-} is an anion (Cl^-, NO_3^-, ClO_4^-, CO_3^{2-}, SO_4^{2-}, $EDTA^{2-}$, etc.). The cations used for LDH synthesis are not limited to divalent and trivalent; ionic radii can also be used: between 0.65 and 0.80 Å for divalent cations and between 0.62 and 0.69 Å for trivalent cations (with the exception of Al, 0.50 Å) [22]. The properties of LDH can be adjusted by changing the divalent and trivalent cations, which affects their physico-chemical properties [23]. Among the most important properties that make hydrotalcite an attractive material in many fields of application are anion exchange and the reconstruction of the calcined materials; these characteristics allow hydrotalcite to act as an adsorbent of anionic organic pollutants by ion exchange or as adsorbents of organic pollutants that would occupy the interlayer space [18, 20, 21].

This work proposes the synthesis of TiO_2-LDH materials using TiO_2 synthesized from titanium butoxide with LDH prepared from Mg-Al, Mg-Fe, and Zn-Al cations as support material. The use of different pairs of cations in the preparation of LDH affects their properties as adsorbent, which in turn has an impact on the photocatalytic behavior of the obtained TiO_2-LDH materials; in addition, we want to know the effect that the different cations used have in the photocatalytic process. The effect of the textural parameters of the obtained materials was also analyzed in relation to their photocatalytic efficiency and adsorption rate, with phenol as the reference organic pollutant.

2. Experimental

2.1. Synthesis of TiO_2 Photocatalyst. TiO_2 was obtained by sol-gel synthesis [8], mixing 90 mL of 1-butanol $C_4H_{10}O$ (Sigma-Aldrich) with 120 mL of deionized water. Both reagents were heated to 70°C in a water bath with continuous agitation and a reflux cooling system. Subsequently, 45 mL of titanium butoxide (TOBX) $C_{16}H_{36}O_4Ti$, 97% (Sigma-Aldrich) was added dropwise. The mixture was aged for 24 hours at constant agitation and temperature maintained with the cooling system. The resulting solid was recovered and washed once with ethanol, dried for 24 hours at 100°C, and finally calcined at 550°C for 3.5 hours.

2.2. Synthesis of $Mg^{2+}Al^{3+}CO_3^{2-}$ LDH. LDH synthesis by the sol-gel method [24] is described as follows: 5.72 g of magnesium ethoxide $C_4H_{10}MgO_2$ (Aldrich) was mixed in 100 mL of ethanol CH_3CH_2OH, 99.5% (Civeq) and 8.8 mL of HCl (Fermont) was added, maintaining the mixture at 80°C with reflux and agitation; a second solution was prepared by dissolving 5.4 g of aluminum acetylacetonate $C_{15}H_{21}AlO_6$ (Aldrich) in 80 mL of ethanol and added dropwise to the first solution maintaining a pH of 10 with a solution of NH_4OH (Aldrich). Finally, 1 mL of water was added. The mixture was aged for 20 hours. The solid was separated by centrifugation, dried at 100°C for 24 hours, and subsequently calcined at 550°C for 3.5 hours.

2.3. Synthesis of $Mg^{2+}Fe^{3+}CO_3^{2-}$ LDH. LDH synthesis by sol-gel with Mg^{2+} and Fe^{3+} as cation layers was obtained by dissolving 5.72 g of magnesium ethoxide in 100 mL of ethanol and adding 8.8 mL of HCl. The solution was maintained at 80°C with reflux and continuous agitation until the magnesium ethoxide was completely dissolved. An aqueous solution was prepared by weighing 6.74 g of ferric nitrate $Fe(NO_3)_3\cdot 9H_2O$ (Meyer) and dissolving it in 80 mL of water. This was then added to the first solution. The pH of the mixture was adjusted to 10 using NH_4OH, adding 1 mL of water. The solution was kept in reflux with constant agitation for 20 hours at 75°C. The resulting solid was separated by centrifugation, dried for 24 hours at 100°C, and calcined at 550°C for 3.5 hours.

2.4. Synthesis of $Zn^{2+}Al^{3+}$ CO_3^{2-} LDH. Sol-gel synthesis with Zn^{2+} and Al^{3+} LDH as cation layers was prepared as follows [25]: 15.84 g of zinc acetylacetonate $C_{10}H_{14}O_4Zn\cdot xH_2O$ (Aldrich) was dissolved in 400 mL of ethanol maintaining the solution at a temperature of 4°C and adding 11 mL of HCl to fully dissolve the zinc acetylacetonate. A second solution was prepared containing 4.12 g of aluminum isopropoxide $C_9H_{21}AlO_3$ (Aldrich) in 100 mL of ethanol and adding 5 mL of HCl for complete dissolution. The zinc solution was then dropped into the aluminum solution and maintained in constant agitation and at a temperature of 4°C. After 3 hours, the pH of the mixture was adjusted to 10 with NaOH 1 M. The solution was agitated at a temperature of 4°C for 15 hours. The resulting gel was separated using centrifugation. The samples were dried for 24 hours at 80°C and calcined at 550°C for 3.5 hours.

2.5. Synthesis of TiO_2-LDH Materials. The preparation of the materials consisted of the mechanical mixing of the TiO_2 solids with each of the different LDH obtained at a weight ratio of 1 : 10. These mixtures of TiO_2 and calcined LDH were mixed in ethanol for 3 hours with vigorous magnetic agitation. The resulting paste was dried at 100°C for 2 hours. The materials were referenced, based on the LDH used, as TiO_2/MgAl, TiO_2/MgFe, and TiO_2/ZnAl.

2.6. Characterization of the Solids. For the XRD analysis, a Bruker Discover D8 diffractometer (Cu k$\alpha\lambda = 1.54$ Å), an intensity of 20 mA, a voltage of 35 kV, scanning speed of 10° (2Θ)/min, and in a 2Θ interval of 10° to 70°, was used. Infrared spectrophotometry analysis was performed using a Varian 640 spectrophotometer in the range 4000 to 500 cm^{-1}. A JEOL 6610LV scanning electron microscope was used for SEM analysis. An Oxford EDS probe was used to perform the elemental chemical analysis. The surface area (SA) was determined by N_2 adsorption using the BET

method on BEL Sorp Max equipment. The data obtained using this technique were used to determine the roughness of the samples by means of fractal dimension.

2.7. Photocatalytic Experiments. The TiO_2/MgAl, TiO_2/MgFe, and TiO_2/ZnAl, in concentrations of 1 g/L, were mixed separately with a phenol solution (Baker) (C_o = 10 mg/L), as well as a solution without any material, to determine the photolytic reaction. Once contact was made, the mixture was agitated and pumped with air for 20 minutes. The mixture was then irradiated with a UV UVS-18 EL (λ = 254 nm, 8 W) lamp for 120 minutes with constant agitation and air pumping. Aliquots were taken during the process to determine the remaining concentrations of phenol by UV-Vis spectrophotometry (λ = 510 nm) using the 4-aminoantipyrine method [26]. The degree of adsorption in the samples was determined by following the procedure described above, without UV-visible irradiation. To verify the recyclability of the photocatalyst, photodegradation experiments were carried out using 10 continuous cycles for each of the materials. The photodegradation cycles were performed as previously described. When one cycle finished, the material was recovered from the solution by sedimentation and a new photodegradation cycle was started with a new phenol solution (C_o = 10 mg/L) until a total of 10 rounds of irradiation were completed. The results were fit to kinetic model of Langmuir-Hinshelwood. All the experiments were conducted in the absence of sunlight and without external pH variation.

3. Results and Discussion

3.1. Characterization

3.1.1. X-Ray Diffraction (XRD). Regarding prepared TiO_2-LDH materials, the diffraction patterns are shown in Figure 1, with reflections mostly related to the anatase phase of TiO_2 (PDF 78-2486) and peaks of lower intensity of TiO_2 brookite (PDF 29-1260), while in TiO_2/MgFe additional minor reflections can be observed associated with the crystallization of magnetite (PDF 87-0245), in TiO_2/ZnAl peaks due to the formation of zincite (PDF 03-0888), and in TiO_2/MgAl a reflection corresponding to MgO crystals (PDF 01-1235) of the calcined LDH component indicative that in the TiO_2/LDH materials the precursors remain segregated [27]. Additionally, a minimum peak intensity is also revealed in all materials due rutile phase (PDF 21-1276) generating materials in the presence of TiO_2 photocatalyst in a mixed anatase-rutile phase, remarking the absence of reflections on the chemical bond between the components.

3.1.2. Infrared Spectroscopy (IR). The spectra presented in Figure 2 for TiO_2-LDH materials show a broadband at 3365 cm^{-1} related to the stretching vibration of the hydroxyl groups of the adsorbed water on their surface [28]. The said band is more noticeable in the TiO_2/MgAl sample. Similarly, common bands of lower intensity associated with the flexion vibration of the O-H groups appear around 1646 cm^{-1}, indicating a minimum quantity of H_2O physically adsorbed into the materials [24–26]. These bands can be more clearly seen

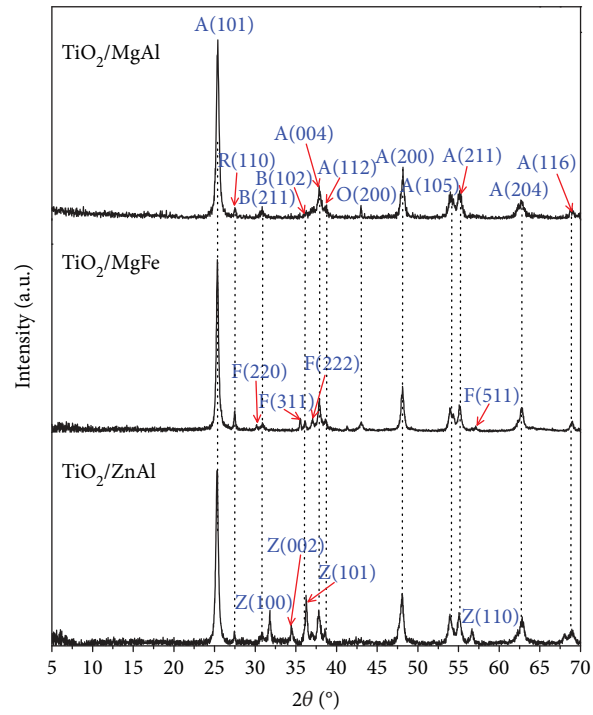

FIGURE 1: XRD patterns for TiO_2/LDH materials with peaks O (periclase), A (TiO_2 anatase), R (TiO_2 rutile), B (TiO_2 brookite), F (magnetite), and Z (zincite).

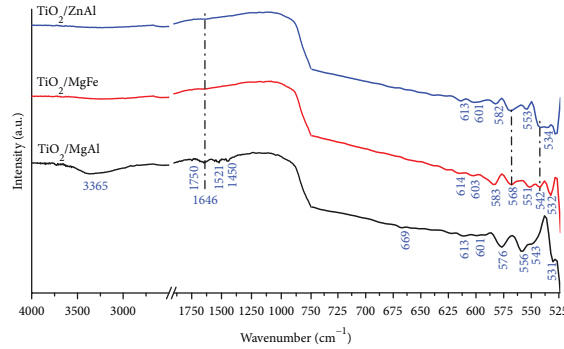

FIGURE 2: IR spectrum for synthesized TiO_2/LDH materials.

in the TiO_2/MgAl sample, indicating higher hydroxylation activity in this material. The vibrations of metal-oxygen bonds related to the different metallic cations used in the synthesis of the LDH components and TiO_2 are presented at lower frequencies, specifically TiO_2/MgAl which presents a band at 699 cm^{-1} due to the vibration of the Mg/Al-OH bond [29]. On the other hand, the bands appearing at frequencies of 614 and 613 cm^{-1} are related to the Ti-O stretching vibration in the isolated TiO_4 tetrahedron [30]; the bands at 603 and 601 cm^{-1} are related to Mg-OH (for TiO_2/MgFe and TiO_2/MgAl, respectively) [31], and the band at 601 cm^{-1} is associated with Zn-OH (for TiO_2/ZnAl) [32]; the bands at 576, 583, and 582 cm^{-1} refer, in this case, to the TiO_2 anatase which tends to vibrate closer to these frequencies [33]. The bands which present at 568 cm^{-1} correspond to the

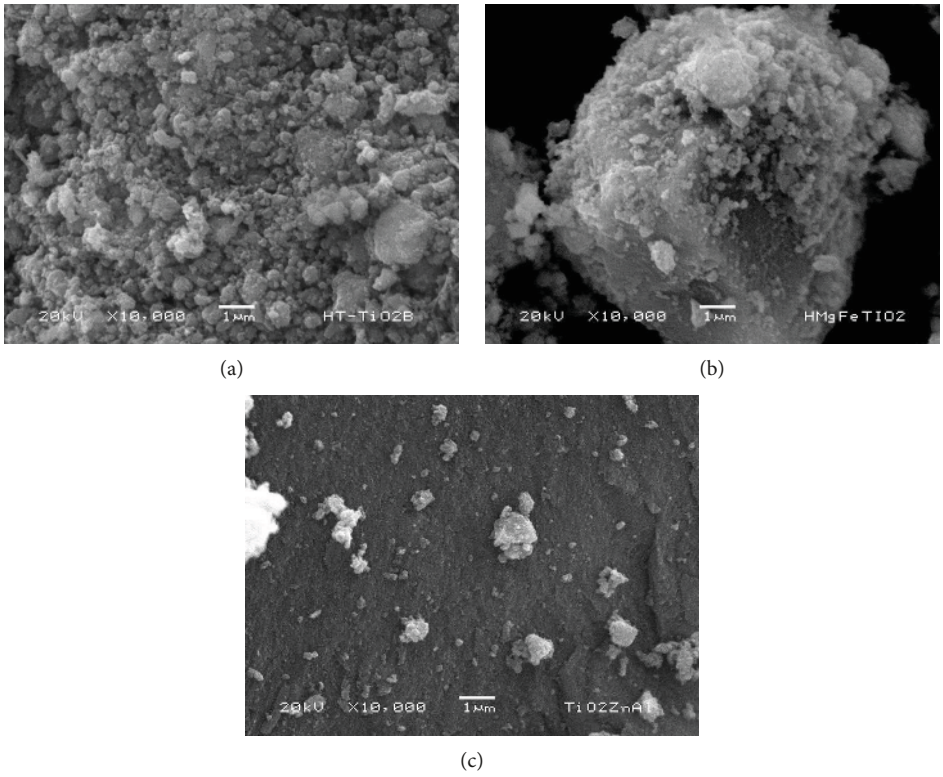

(a) (b) (c)

Figure 3: Micrographs for the TiO_2-LDH materials (a) TiO_2/MgAl, (b) TiO_2/MgFe, and (c) TiO_2/ZnAl.

metal-oxygen vibrations of the Zn-O [32, 34] and Fe-O [35] molecules. The bands at 556, 551, and 553 cm^{-1} are related to the symmetric stretching vibration of Ti-O-Ti [33, 36], while the bands at 543 and 542 cm^{-1} are associated with the Ti-O vibration of the condensed octahedron of the TiO_6 molecule [30], whereas the group of bands at 531, 532, and 534 cm^{-1} can be associated with the Ti-O vibration of rutile TiO_2 [33].

3.1.3. Scanning Electron Microscopy (SEM). Figure 3 shows the micrographs for the different synthesized materials; mechanical mixing of hydrotalcites and TiO_2 precursors results in no chemical bonding between the components, maintained separate phases of materials [37]; the SEM micrographs present a combination of particles of the component precursors which is corroborated in the EDS analysis presented in Table 1. The TiO_2/MgAl and TiO_2/MgFe samples show a particle morphology of quite dense irregularly arranged agglomerates of nanometric particles due to the sol gel synthesis applied to these materials [38]. On the other hand, the TiO_2/ZnAl particles are more differentiated, the smallest particles of the photocatalyst being exposed to a large extent on the surface of the larger particles of the LDH component, which appear more homogeneous and smooth, causing greater photocatalytic activity in this specific material, as will be seen later in the photocatalytic tests.

3.2. BET Analysis

3.2.1. Surface Area (SA). The textural properties of a photocatalyst affect its contact with pollutants. The heterogeneous photocatalytic degradation process produces better yields in photocatalysts with high surface area and pore volume, which increases the likelihood that the pollutant molecules and their oxidation intermediates come into direct contact with the photogenerated holes, thereby increasing the photodegradation process [5]. Table 2 shows the results of the textural analysis of the synthesized solids.

Table 1: Analysis EDS for TiO_2-LDH materials (atomic %).

Element	TiO_2/MgAl	TiO_2/MgFe	TiO_2/ZnAl
C	10.7	4	8.1
O	55.9	61.4	53
Mg	1.8	4.6	—
Al	0.7	—	1.7
Fe	—	2	—
Zn	—	—	4.9
Ti	30.9	28	32.3

The hysteresis loop in adsorption-desorption isotherms is due to the difference between the pore filling pressure and emptying pressure during the BET gas adsorption process to determine the surface area. This is a characteristic of materials with a porous structure [39]. The isotherms obtained for the materials presented in Figure 4 are observed to be of type IV, according to IUPAC classification [40]. Type IV isotherms describe a multilayer adsorption process reflected in a central zone of the isotherm, rising as more layers are absorbed on the surface of solid. As

Table 2: BET surface area, total pore volume, and average pore diameter for TiO_2-LDH materials.

Sample	Surface area (m^2/g)	Pore total volume (cm^3/g) ($\times 10^{-2}$)	Pore medium diameter (nm)	Fractal dimension
TiO_2/MgAl	45.29	11.12	9.82	2.14
TiO_2/MgFe	49.34	15.53	12.59	2.11
TiO_2/ZnAl	47.53	12.27	10.33	2.08

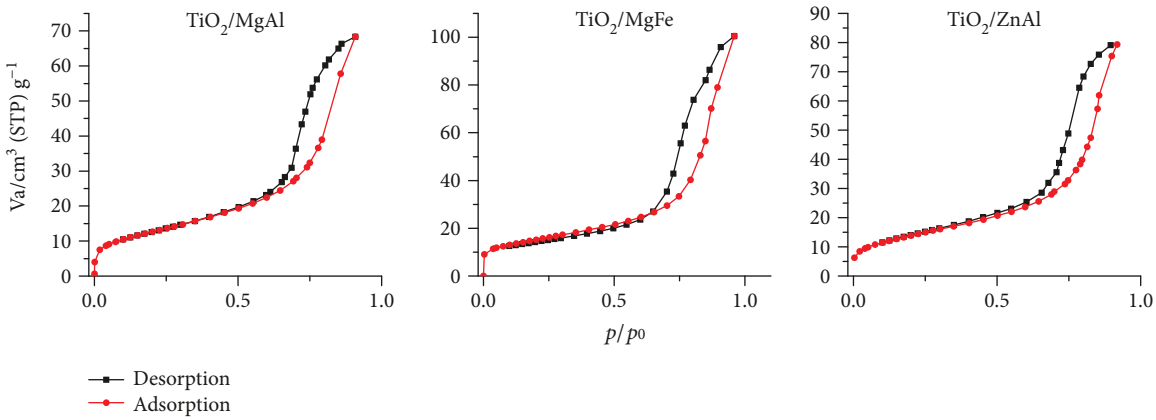

Figure 4: Adsorption-desorption N_2 isotherms for TiO_2/LDH materials.

it nears saturation pressure, the slope of the isotherm decreases until reaching equilibrium. The hysteresis loop presented by the material isotherms is associated with type D (H3), representative of the capillary geometries in the form of variable-width sheets open at both ends. This type of hysteresis is usually found in materials that form particle aggregates which indicate the presence of slit-like pores [41], typical of layered materials like LDH [28]. The isotherms are used to calculate the textural parameters of the materials (BET surface area, total pore volume, and average pore diameter), which are also shown in Table.

The results for the synthesized TiO_2/LDH materials show smaller surface areas than those reported for LDH-type materials [20], falling into the range of 45.29–49.34 m^2/g. This is attributed to the contribution of the photocatalyst TiO_2, which has smaller surface areas, the reduction in pore volume due to heat treatment, and the presence of Fe and Zn oxides in the materials, which have smaller surface areas compared to LDH. The results for total pore volume are in direct relation to the values for surface area, as are the values for average pore diameter, which are in the range from 9.82 to 12.59 nm, associated with mesoporous materials (2 nm < average pore diameter < 50 nm) [42].

3.2.2. Determination of Surface Fractal Dimension (D). Surface fractal dimension (D) can be determined by following the Frenkel–Halsey–Hill (FHH) equation [11, 39]:

$$\ln\left(\frac{V}{\mathrm{Vm}}\right) = K + a * \left(\ln\left(\ln\left(\frac{p_0}{p}\right)\right)\right), \quad (1)$$

where V is the volume of gas in standard conditions of temperature and pressure, Vm is the volume of the monolayer, p is the equilibrium pressure and p_0 is the saturation pressure of the adsorbate. Plotting $\ln(V/\mathrm{Vm})$ against $\ln(\ln(p_0/p))$, slope a takes the value of $(D_1 - 3)/3$ when Van der Waals forces (low coverage) are dominant during the adsorption process at the solid-gas interface and the slope obtained is greater than −1/3. On the other hand, slope a is considered as $D_1 - 3$ when the interface is controlled by gas-liquid tension (capillary force or high coverage), causing the interface to move away from the surface, reducing the interface area, and the slope obtained is less than −1/3, thus enabling the calculation of the fractal dimension [43].

The linearized graphs obtained from the N_2 adsorption data are presented in Figure 5; the respective linear equations were obtained with an $R^2 > 0.99$. The adsorption technique used reveals the existence of fractal properties; the results of the surface fractal dimension calculations using the data of the adsorption isotherms are also included in the table. The surface fractal dimension (D) values obtained for the TiO_2/LDH materials are in the range of 2.08 to 2.14, indicating that the surface geometry of those materials tends to be slightly rough, in addition to the mesoporous nature of the analyzed samples.

The roughness of a surface is due to the presence of uniform pores or the existence of wide pore-size distribution [44]. The analysis of the results reveals a relationship between the calculated fractal dimension values and the width of the hysteresis loops of the adsorption isotherms for each of the materials analyzed (Figure 6), which are associated with the pore-size distribution. This leads us to establish a dependence in the synthesized materials between roughness and structural heterogeneity [11] where in the case of materials with greater pore-size distribution (associated with a wider

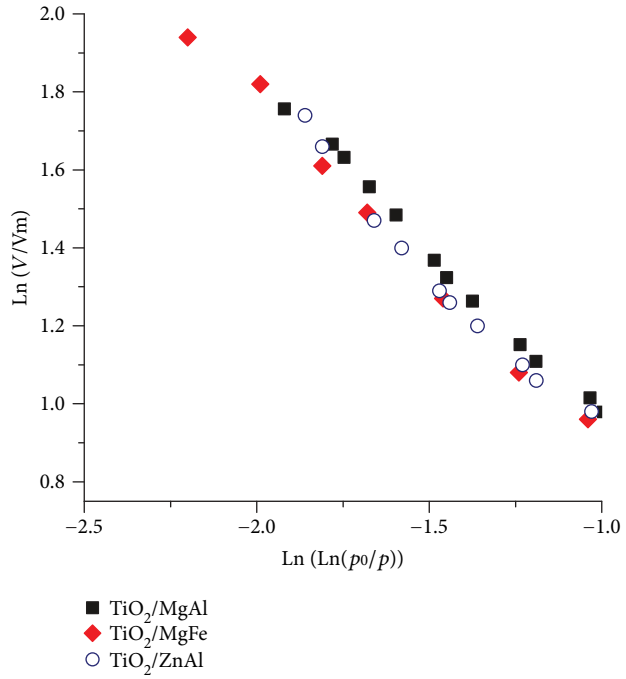

Figure 5: Linearization of N_2 adsorption isotherms using the Frenkel–Halsey–Hill equation for TiO_2/LDH materials.

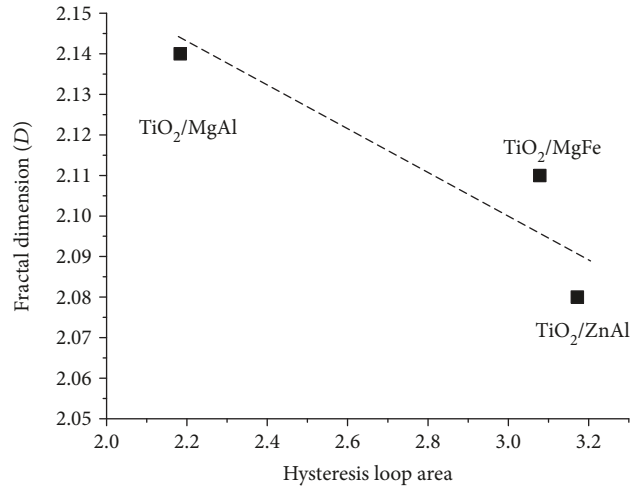

Figure 6: Relationship between pore-size distribution and fractal dimension for TiO_2/LDH materials.

hysteresis cycle), a lower fractal dimension value was obtained compared to the materials with a narrower hysteresis loop. Consequently, the roughness of these materials is associated more with the presence of uniform pores than wide pore-size distribution.

3.3. Photocatalytic Experiments. In heterogeneous photocatalysis processes, several phenomena can occur: on the one hand, direct photodegradation is where the adsorption of the organic pollutant on the surface of the catalyst enhances decomposition by the photogenerated holes. On the other hand, the indirect photodegradation mechanism is based on the formation of $^{\cdot}OH$ radicals by photocatalyst excitation which react with the organic material, degrading it. Other processes that can occur in phenol photodegradation might be direct photolysis due to the presence of UV radiation and photooxidation due to the action of the UV radiation and the oxidizing agent but without participation from the photocatalyst [5].

The photodegradation curves for the TiO_2/LDH materials are shown in Figure 7. The adsorption capacity of the materials (Figure 7(a)) is lower than the photocatalytic capacity, achieving phenol removal after 120 minutes of UV radiation of 3.2, 14.6, and 15.0% for TiO_2/MgAl, TiO_2/MgFe, and TiO_2/ZnAl, respectively, compared to the original concentration. Phenol removal is higher in the last two materials in which the cation pairs MgFe and ZnAl were used as precursors, since there is a more favorable interaction between the surface of the material and phenol, achieving greater adsorption of the pollutant.

The photodegradation curves (Figure 7(b)), in general, show slightly higher photocatalytic activity during the first minutes of reaction, when there is less competition between the phenol molecules to degrade. This happens because, as the minutes pass, the photodegradation intermediates limit direct phenol removal by the photocatalyst while competing for the $^{\cdot}OH$ radicals that are formed, slightly flattening the curves, but maintaining photodegradation. The photodegradation percentages obtained for the TiO_2/MgAl, TiO_2/MgFe, and TiO_2/ZnAl materials are 49.8, 43.3, and 55.7%, respectively (slightly higher than the rate of 46.2% obtained with the original TiO_2 precursor), while photolytic reaction reaches 11.0% of phenol photodegradation. Less photoactivity is observed in TiO_2/MgFe, associated with the presence of Fe^{3+} ions since they can affect water transmittance and act as $^{\cdot}OH$ radical scavengers due to the capture of conduction band electrons by the metal ions [45], whereas the presence of Zn in the TiO_2/ZnAl sample caused greater photoactivity attributed to the fact that, like TiO_2, zinc oxides have photocatalytic properties [46] that enhance the catalytic activity in this material. On the other hand, the TiO_2/MgAl material, despite having low adsorption rates, did not result in a reduction in photoactivity.

These results confirm, on the one hand, that phenol removal is largely attributed to the photodegradation process, ruling out the concurrence of adsorption and photolysis phenomena, since the removal percentages of the latter are significantly lower than those reached in the photocatalytic reaction. In addition, phenol photodegradation in these materials is mainly attributed to indirect photocatalysis by the formation of $^{\cdot}OH$ radicals, as opposed to direct photodegradation caused by photogenerated holes.

3.3.1. Kinetic Model of Langmuir-Hinshelwood (L-H). The L-H kinetic model considers that the reaction rate (r) is proportional to the fraction of the surface covered by the pollutant [18, 28]. When the concentration of the solution (C) is highly diluted ($C < 10^{-3}$ mol/L) and when the adsorption of the contaminant is relatively weak, this our

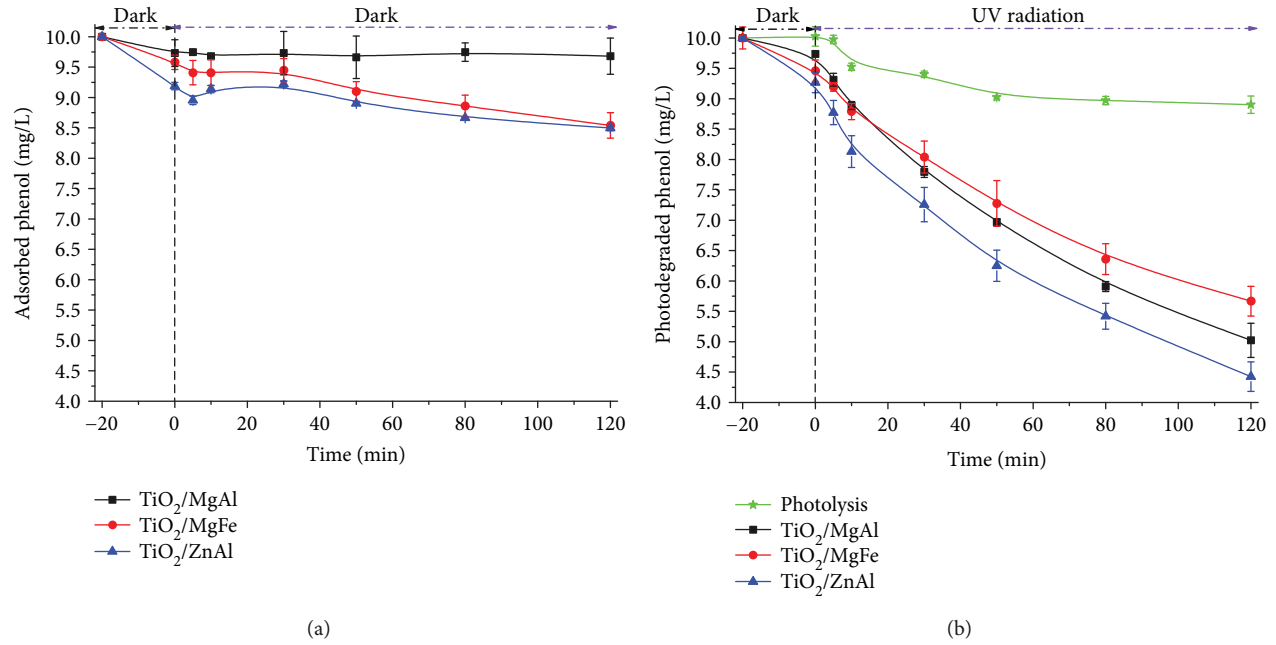

FIGURE 7: Phenol adsorption and photodegradation with TiO_2-LDH materials (a) adsorbed and (b) photodegraded.

case ($C_{phenol} = 1.063 \times 10^{-4}$ mol/L), the degradation follows a pseudo-first order reaction:

$$r = -\frac{dC}{dt} = k_{ap}C, \tag{2}$$

where $k_{ap}$is the apparent rate constant of a pseudo-first order reaction. Simplifying equation 2 to a first-order reaction, we have

$$\ln\left(\frac{C_o}{C}\right) = k_{ap}t. \tag{3}$$

Plotting ln (C_o/C) against time (t), the apparent rate constant (k_{ap}) can be determined by the slope of the curve obtained [18, 28]. Figure 8 shows the results of the kinetic study on the degradation of phenol with the TiO_2/LDH materials. Additionally, the results obtained with the commercial sample Evonik Aeroxide are shown.

The parameters k_{ap}, $t_{1/2}$ (is the time required to degrade the phenol half), and the linear correlation adjustment r obtained for the samples evaluated are listed in Table 3. The k_{ap} value in the samples is according to the following order: TiO_2/ZnAl > TiO_2/MgAl > TiO_2-Evonik > TiO_2/MgFe; this relationship corresponds with the percentages of photodegradation obtained for each of the samples.

3.3.2. Reuse of Materials. The results obtained by reusing the same solid from the synthesized materials in 10 cycles are shown in Figure 9. The combination of the photocatalyst with the LDH allowed the separation of the materials, which was carried out by sedimentation of the solid without any external intervention from the irradiated aqueous solution obtaining, after one cycle, a weight loss in the solid of 8 ± 3% due to the loss of material while taking the aliquots

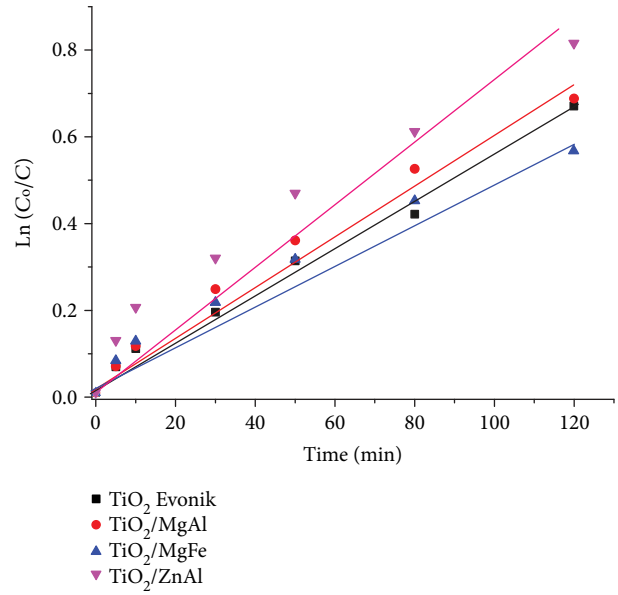

FIGURE 8: Pseudo-first order kinetics for adjustment to model Langmuir-Hinshelwood.

TABLE 3: Kinetic parameters obtained for Langmuir-Hinshelwood model.

Sample	k_{ap} *(mg/L·min)*	$t_{1/2}$ *(min)*	r^2
TiO_2 Evonik©	5.2×10^{-3}	133.2975	0.9912
TiO_2/MgAl	5.5×10^{-3}	126.0268	0.9882
TiO_2/MgFe	4.3×10^{-3}	161.1970	0.9861
TiO_2/ZnAl	6×10^{-3}	115.5245	0.9849

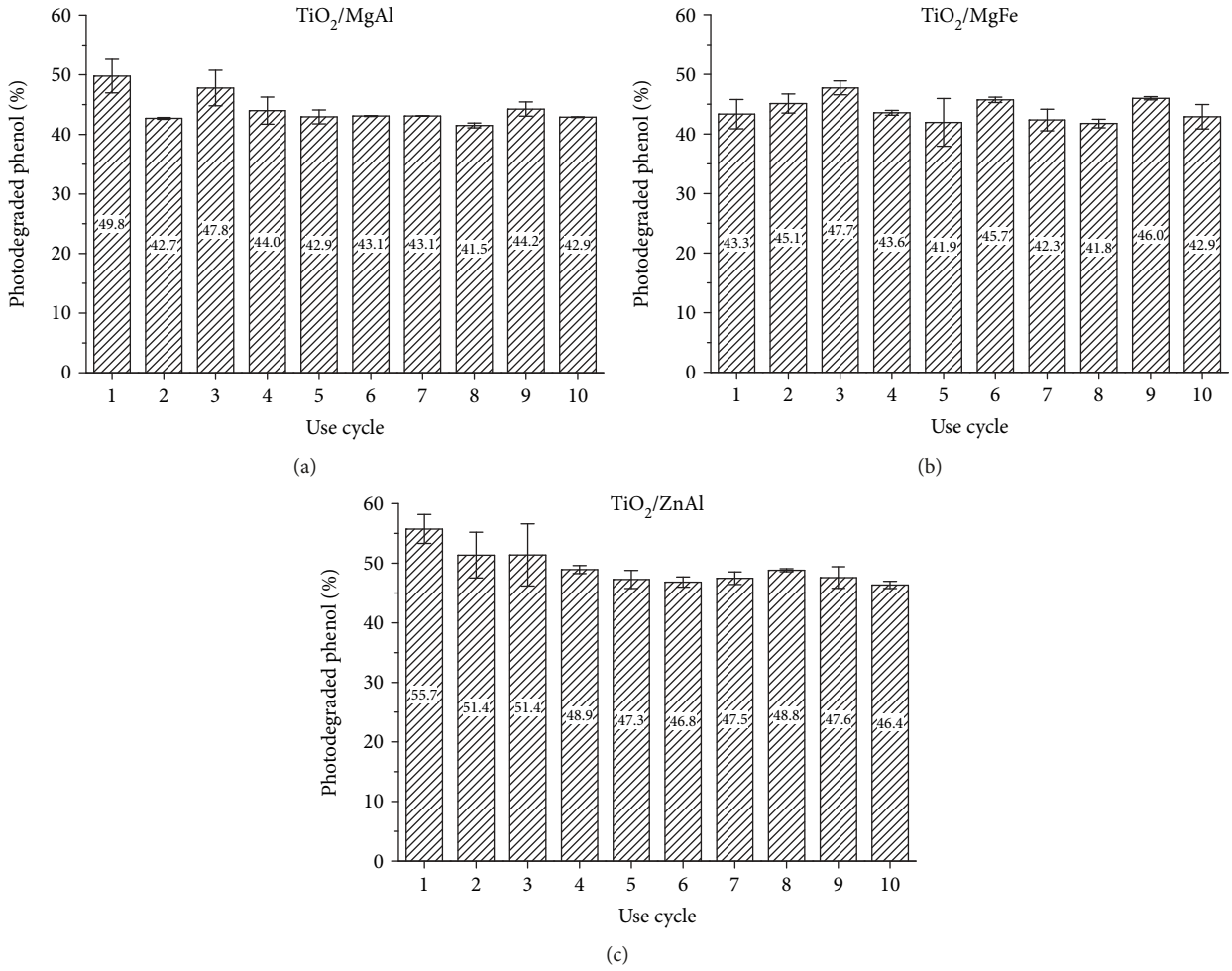

Figure 9: Reuse of TiO_2-LDH materials.

during UV radiation; this loss was compensated by the addition of new material to recover the original concentration of the solid (1 g/L). Synergy is observed between the components of the materials which, once they form it, do not lose their properties, enabling them to be reused in a photodegradation cycle. The results show that the photocatalytic capacity of the materials is maintained without further decreasing degradation efficiency. The decline in photocatalytic activity in successive photodegradation cycles is not generally significant and, in this case, is attributed to low TiO_2 deactivation due to its high photochemical resistance [47].

TiO_2/MgAl showed an average decrease in efficiency of 5.9% at the end of the 10 photodegradation cycles, whereas there appears to be no deactivation when using TiO_2/MgFe, registering only a minimal loss (0.4%) of photocatalytic activity. Meanwhile, a 9.3% reduction in efficiency is observed for TiO_2/ZnAl, attributed to its minimal ZnO fraction, which has a greater tendency to photocorrosion under UV radiation compared to TiO_2 [48]. However, the materials do not undergo decomposition, retaining their properties of sedimentation and easy recovery after use.

The contour charts presented in Figure 10 analyze the relationship between the textural parameters of TiO_2/LDH materials and their photocatalytic and phenol adsorption properties. In the specific case of surface area, values higher than 48 m^2/g produced higher adsorption percentages, coinciding with lower photodegradation percentages, while maximum photodegradation efficiency is reached in the range below 48 m^2/g.

On the other hand, surface roughness expressed in terms of the fractal dimension has an effect on the photocatalytic and adsorption parameters, finding that less rough surfaces ($2.080 < D < 2.095$) tend to produce materials with greater adsorption capacity, while higher photodegradation efficiency is obtained by increasing the surface roughness of the materials, gradually decreasing their adsorptive capacity but without altering their photocatalytic capacity.

The structural heterogeneity of the samples, in terms of pore-size distribution [44], has a direct influence on the adsorption capacity of the materials; the tendency indicates that a greater pore-size distribution (larger area of the hysteresis loop) benefits the phenol adsorption process, while the photocatalytic capacity of the materials is not affected until the point where structural homogeneity appears to be reached (hysteresis area < 2.20). After this point, the adsorption process is minimized and the photocatalytic capacity is limited to intermediate values compared to those reported, as shown in the contour chart in Figure 10.

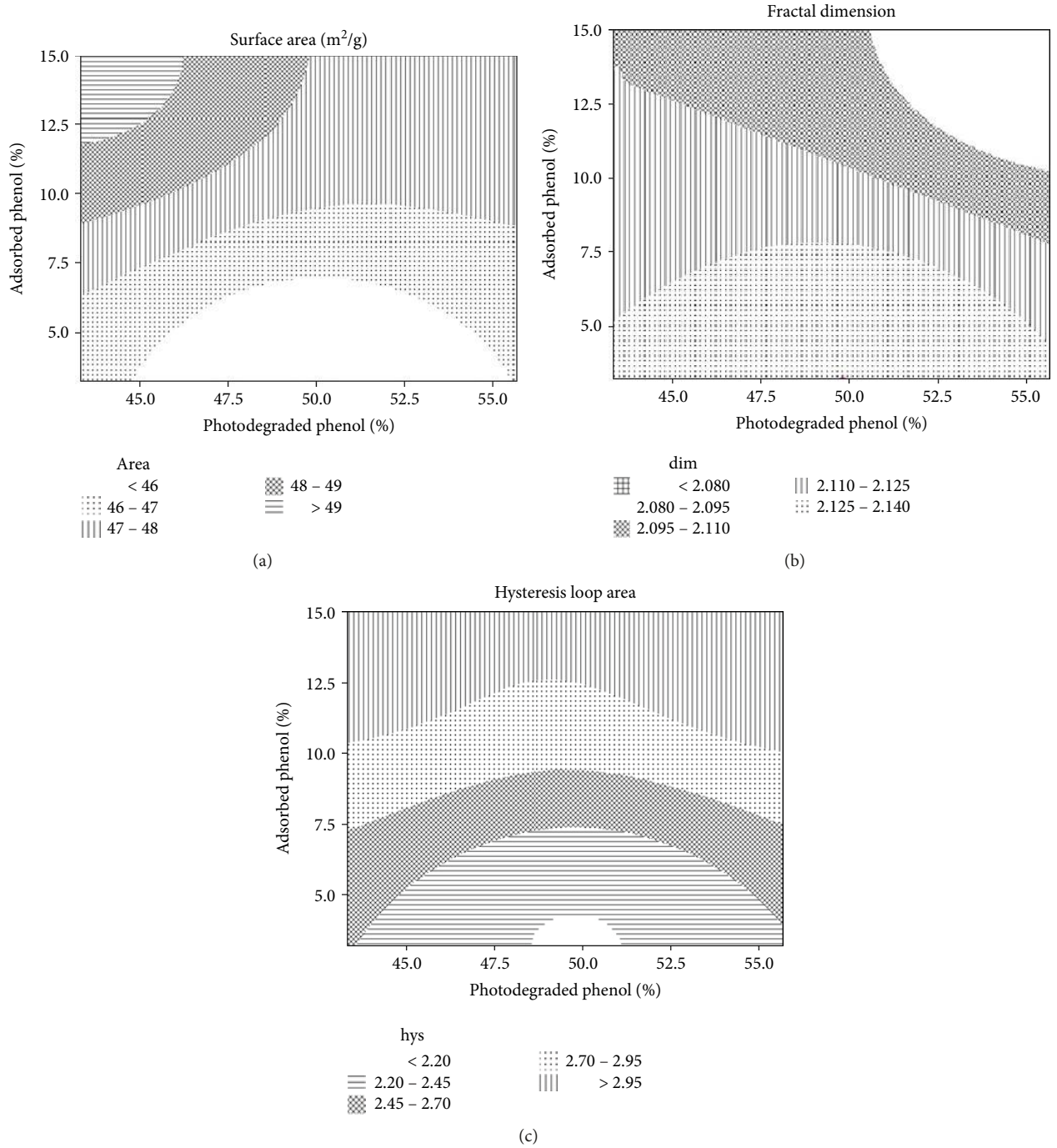

Figure 10: Relation between the textural parameters of the materials and their adsorption and phenol photodegradation capacities.

Based on these results, the most suitable values for textural parameters (surface area, surface roughness, and pore-size distribution) are at an intermediate level, in which the adsorption and phenol photodegradation capacity is not compromised; whereas with extreme values of these parameters, one phenol removal process may benefit while another is minimized.

4. Conclusions

Materials derived from TiO_2 and LDH were synthesized, the latter prepared with MgAl, MgFe, and ZnAl cation pairs, exhibiting phenol adsorption and degradation properties. The use of the different cations of the LDH component produced materials with different photocatalytic and phenol adsorption capacities; TiO_2/ZnAl was found to achieve the highest level of phenol adsorption and photodegradation. However, the results of the material reuse tests showed that TiO_2/ZnAl underwent the greatest photocatalytic deactivation after 10 cycles of use. Minimal photocatalytic deactivation was observed with TiO_2/MgFe, while intermediate photo-deactivation was seen with TiO_2/MgAl. In addition, the differences in textural characteristics presented by the

materials affected their phenol adsorption and photodegradation efficiency, finding that intermediate values of textural parameters (surface area, surface roughness, and pore-size distribution) do not compromise adsorption capacity and phenol degradation, while extreme values of the said parameters are detrimental to some of the phenol removal processes.

Data Availability

The data used to support the findings of this study are included within the article.

Conflicts of Interest

The authors declare that they have no conflicts of interest.

Acknowledgments

J.C. Contreras-Ruiz acknowledges a Scholarship from CONACYT-México and thanks financial support (CVU 493858).

References

[1] S. Ahmed, M. G. Rasul, W. N. Martens, R. Brown, and M. A. Hashib, "Heterogeneous photocatalytic degradation of phenols in wastewater: a review on current status and developments," *Desalination*, vol. 261, no. 1-2, pp. 3–18, 2010.

[2] W. Nawawi, R. Zaharudin, M. Ishak, K. Ismail, and A. Zuliahani, "The preparation and characterization of immobilized TiO_2/PEG by using DSAT as a support binder," *Applied Sciences*, vol. 7, no. 1, 2017.

[3] S. Afshar, H. Samari Jahromi, N. Jafari, Z. Ahmadi, and M. Hakamizadeh, "Degradation of malachite green oxalate by UV and visible lights irradiation using $Pt/TiO_2/SiO_2$ nanophotocatalyst," *Scientia Iranica*, vol. 18, no. 3, pp. 772–779, 2011.

[4] M. R. Hoffmann, S. T. Martin, W. Choi, and D. W. Bahnemann, "Environmental applications of semiconductor photocatalysis," *Chemical Reviews*, vol. 95, no. 1, pp. 69–96, 1995.

[5] H. Kisch, *Semiconductor Photocatalysis: Principles and Applications*, Wiley, 2015.

[6] S. Bagheri, K. Shameli, and S. B. Abd Hamid, "Synthesis and characterization of anatase titanium dioxide nanoparticles using egg white solution via sol-gel method," *Journal of Chemistry*, vol. 2013, Article ID 848205, 5 pages, 2013.

[7] D. Huang, Y. Miyamoto, T. Matsumoto et al., "Preparation and characterization of high-surface-area TiO_2/activated carbon by low-temperature impregnation," *Separation and Purification Technology*, vol. 78, no. 1, pp. 9–15, 2011.

[8] J. Araña, A. P. Alonso, J. M. D. Rodríguez, G. Colón, J. A. Navío, and J. P. Peña, "FTIR study of photocatalytic degradation of 2-propanol in gas phase with different TiO_2 catalysts," *Applied Catalysis B: Environmental*, vol. 89, no. 1-2, pp. 204–213, 2009.

[9] A. Ahmad, G. Hamed, and A. Salman, "Synthesis and applications of TiO_2 nanoparticles," *Pakistan Engineeering Congress, 70th Annual Session Proceedings*, vol. 70, no. 676, pp. 403–412, 2007.

[10] S.-H. Lin, C.-H. Chiou, C.-K. Chang, and R.-S. Juang, "Photocatalytic degradation of phenol on different phases of TiO_2 particles in aqueous suspensions under UV irradiation," *Journal of Environmental Management*, vol. 92, no. 12, pp. 3098–3104, 2011.

[11] J. C. Contreras-Ruiz, M. S. Martínez-Gallegos, and E. Ordoñez-Regil, "Surface fractal dimension of composites TiO_2-hydrotalcite," *Materials Characterization*, vol. 121, pp. 17–22, 2016.

[12] V. Durgakumari, M. Subrahmanyam, K. V. Subba Rao, A. Ratnamala, M. Noorjahan, and K. Tanaka, "An easy and efficient use of TiO_2 supported HZSM-5 and TiO_2+HZSM-5 zeolite combinate in the photodegradation of aqueous phenol and *p* -chlorophenol," *Applied Catalysis A: General*, vol. 234, no. 1-2, pp. 155–165, 2002.

[13] N. Bayal and P. Jeevanandam, "Synthesis of TiO_2-MgO mixed metal oxide nanoparticles via a sol-gel method and studies on their optical properties," *Ceramics International*, vol. 40, no. 10, pp. 15463–15477, 2014.

[14] P. S. Yap, Y. L. Cheah, M. Srinivasan, and T. T. Lim, "Bimodal N-doped P25-TiO_2/AC composite: preparation, characterization, physical stability, and synergistic adsorptive-solar photocatalytic removal of sulfamethazine," *Applied Catalysis A: General*, vol. 427-428, pp. 125–136, 2012.

[15] L. Zhang and Y. Zhang, "Adsorption characteristics of hexavalent chromium on HCB/TiO_2," *Applied Surface Science*, vol. 316, no. 1, pp. 649–656, 2014.

[16] Z. Huang, P. Wu, Y. Lu, X. Wang, N. Zhu, and Z. Dang, "Enhancement of photocatalytic degradation of dimethyl phthalate with nano-TiO_2 immobilized onto hydrophobic layered double hydroxides: a mechanism study," *Journal of Hazardous Materials*, vol. 246-247, pp. 70–78, 2013.

[17] E. M. Seftel, M. Niarchos, C. Mitropoulos, M. Mertens, E. F. Vansant, and P. Cool, "Photocatalytic removal of phenol and methylene-blue in aqueous media using TiO_2@LDH clay nanocomposites," *Catalysis Today*, vol. 252, pp. 120–127, 2015.

[18] J. Prince, F. Tzompantzi, G. Mendoza-Damián, F. Hernández-Beltrán, and J. S. Valente, "Photocatalytic degradation of phenol by semiconducting mixed oxides derived from Zn(Ga)Al layered double hydroxides," *Applied Catalysis B: Environmental*, vol. 163, pp. 352–360, 2015.

[19] S. P. Paredes, M. A. Valenzuela, G. Fetter, and S. O. Flores, "TiO_2/MgAl layered double hydroxides mechanical mixtures as efficient photocatalysts in phenol degradation," *Journal of Physics and Chemistry of Solids*, vol. 72, no. 8, pp. 914–919, 2011.

[20] J. C. Contreras-Ruiz, S. Martínez-Gallegos, E. Ordoñez, J. C. González-Juárez, and J. L. García-Rivas, "Synthesis of hydroxide–TiO_2 compounds with photocatalytic activity for degradation of phenol," *Journal of Electronic Materials*, vol. 46, no. 3, pp. 1658–1668, 2017.

[21] F. M. Fernandes, H. Baradari, and C. Sanchez, "Integrative strategies to hybrid lamellar compounds: an integration challenge," *Applied Clay Science*, vol. 100, pp. 2–21, 2014.

[22] C. Forano, U. Costantino, V. Prévot, and C. T. Gueho, *Layered Double Hydroxides (LDH)*, vol. 5, Faiza Bergaya, Gerhard Lagaly Editors, Elsevier, 2013.

[23] F. Bellezza, M. Nocchetti, T. Posati, S. Giovagnoli, and A. Cipiciani, "Synthesis of colloidal dispersions of NiAl, ZnAl, NiCr, ZnCr, NiFe, and MgFe hydrotalcite-like nanoparticles,"

Journal of Colloid and Interface Science, vol. 376, no. 1, pp. 20–27, 2012.

[24] J. S. Valente, E. Lima, J. A. Toledo-Antonio et al., "Comprehending the thermal decomposition and reconstruction process of sol-gel MgAl layered double hydroxides," *Journal of Physical Chemistry C*, vol. 114, no. 5, pp. 2089–2099, 2010.

[25] D. Tichit, O. Lorret, B. Coq, F. Prinetto, and G. Ghiotti, "Synthesis and characterization of Zn/Al and Pt/Zn/Al layered double hydroxides obtained by the sol-gel method," *Microporous and Mesoporous Materials*, vol. 80, no. 1–3, pp. 213–220, 2005.

[26] J. Rodier, B. Legube, and N. Merlet, *Análisis del Agua*, Omega, Barcelona, 2010.

[27] E. M. Seftel, M. Niarchos, N. Vordos et al., "LDH and TiO_2/LDH-type nanocomposite systems: a systematic study on structural characteristics," *Microporous and Mesoporous Materials*, vol. 203, pp. 208–215, 2015.

[28] Z. Bouberka, K. A. Benabbou, A. Khenifi, and U. Maschke, "Degradation by irradiation of an acid orange 7 on colloidal TiO_2/(LDHs)," *Journal of Photochemistry and Photobiology A: Chemistry*, vol. 275, pp. 21–29, 2014.

[29] Z. P. Xu and P. S. Braterman, "Synthesis, structure and morphology of organic layered double hydroxide (LDH) hybrids: comparison between aliphatic anions and their oxygenated analogs," *Applied Clay Science*, vol. 48, no. 1-2, pp. 235–242, 2010.

[30] M. Crisan, A. Jitianu, M. Zaharescu, F. Mizukami, and S. Niwa, "Sol-gel mono- and poly-component nanosized powders in the Al_2O_3–TiO_2–SiO_2–MgO system," *Journal of Dispersion Science and Technology*, vol. 24, no. 1, pp. 129–144, 2007.

[31] T. López, P. Bosch, M. Asomoza, R. Gómez, and E. Ramos, "DTA-TGA and FTIR spectroscopies of sol-gel hydrotalcites: aluminum source effect on physicochemical properties," *Materials Letters*, vol. 31, no. 3-6, pp. 311–316, 1997.

[32] G. Carja, A. Nakajima, S. Dranca, C. Dranca, and K. Okada, "TiO_2/ZnLDH as a self-assembled nanocomposite with photoresponsive properties," *Journal of Physical Chemistry C*, vol. 114, no. 35, pp. 14722–14728, 2010.

[33] L. I. Myronyuk, I. F. Myronyuk, V. L. Chelyadyn et al., "Structural and morphological features of crystalline nanotitania synthesized in different aqueous media," *Chemical Physics Letters*, vol. 583, pp. 103–108, 2013.

[34] A. A. A. Ahmed, Z. A. Talib, and M. Z. Hussein, "Synthesis and optimization of electric conductivity and thermal diffusivity of zinc-aluminum hydroxide (Zn–Al–NO_3–LDH) prepared at different pH values," *Applied Catalysis A: General*, vol. 3, no. 2, pp. 130–144, 2016.

[35] S. Mohapatra, N. Pramanik, S. Mukherjee, S. K. Ghosh, and P. Pramanik, "A simple synthesis of amine-derivatised superparamagnetic iron oxide nanoparticles for bioapplications," *Journal of Materials Science*, vol. 42, no. 17, pp. 7566–7574, 2007.

[36] W. Sangchay, L. Sikong, and K. Kooptarnond, "Comparison of photocatalytic reaction of commercial P25 and synthetic TiO_2-AgCl nanoparticles," *Procedia Engineering*, vol. 32, pp. 590–596, 2012.

[37] J. C. Contreras-Ruiz, S. Martínez-Gallegos, J. L. García-Rivas, J. C. González-Juárez, and E. Ordoñez, "Influence of the synthesis method on the preparation composites derived from TiO_2-LDH for phenol photodegradation," in *Titanium Dioxide-Material for a Sustainable Environment*, D. Yang, Ed., InTech, 2018.

[38] N. Chubar, V. Gerda, O. Megantari et al., "Applications versus properties of Mg-Al layered double hydroxides provided by their syntheses methods: alkoxide and alkoxide-free sol-gel syntheses and hydrothermal precipitation," *Chemical Engineering Journal*, vol. 234, pp. 284–299, 2013.

[39] J. Rouquerol, D. Avnir, C. W. Fairbridge et al., "Recommendations for the characterization of porous solids (technical report)," *Pure and Applied Chemistry*, vol. 66, no. 8, pp. 1739–1758, 1994.

[40] B. Kosata, M. Nic, and J. Jirat, *IUPAC Compendium of Chemical Terminology*, IUPAC Gold Book, 2014.

[41] M. Thommes, K. Kaneko, A. V. Neimark et al., "Physisorption of gases, with special reference to the evaluation of surface area and pore size distribution (IUPAC technical report)," *Pure and Applied Chemistry*, vol. 87, no. 9-10, pp. 1051–1069, 2015.

[42] J. Vilchis-Granados, F. Granados-Correa, and C. E. Barrera-Díaz, "Surface fractal dimensions and textural properties of mesoporous alkaline-earth hydroxyapatites," *Applied Surface Science*, vol. 279, pp. 97–102, 2013.

[43] P. Pfeifer, Y. J. Wu, M. W. Cole, and J. Krim, "Multilayer adsorption on a fractally rough surface," *Physical Review Letters*, vol. 62, no. 17, pp. 1997–2000, 1989.

[44] G. M. S. El Shafei, C. A. Philip, and N. A. Moussa, "Fractal analysis of hydroxyapatite from nitrogen isotherms," *Journal of Colloid and Interface Science*, vol. 277, no. 2, pp. 410–416, 2004.

[45] A. K. Aboul-Gheit, D. S. El-Desouki, and R. A. El-Salamony, "Different outlet for preparing nano-TiO_2 catalysts for the photodegradation of black B dye in water," *Egyptian Journal of Petroleum*, vol. 23, no. 3, pp. 339–348, 2014.

[46] A. Kolodziejczak-Radzimska and T. Jesionowski, "Zinc oxide-from synthesis to application: a review," *Materials*, vol. 7, no. 4, pp. 2833–2881, 2014.

[47] H. Kisch, "On the problem of comparing rates or apparent quantum yields in heterogeneous photocatalysis," *Angewandte Chemie International Edition*, vol. 49, no. 50, pp. 9588-9589, 2010.

[48] X. Xiang, L. Xie, Z. Li, and F. Li, "Ternary MgO/ZnO/In_2O_3 heterostructured photocatalysts derived from a layered precursor and visible-light-induced photocatalytic activity," *Chemical Engineering Journal*, vol. 221, pp. 222–229, 2013.